Fabrication and Evaluation of Solution-Processed Reduced Graphene Oxide Electrodes for p- and n-Channel Bottom-Contact Organic Thin-Film Transistors

Héctor A. Becerril,[†,‡] Randall M. Stoltenberg,[†] Ming Lee Tang,[†] Mark E. Roberts,[†] Zunfeng Liu,[§] Yongsheng Chen,[§] Do Hwan Kim,[⊥] Bang-Lin Lee,[⊥] Sangyoon Lee,[⊥] and Zhenan Bao[†,*]

[†]Department of Chemical Engineering, Stanford University, Stanford, California 94305, United States, [‡]Department of Chemistry, Brigham Young University-Idaho, Rexburg, Idaho 83440, United States, [§]Key Laboratory for Functional Polymer Materials and Center for Nanoscale Science and Technology, College of Chemistry, Institute of Polymer Chemistry, Nankai University, Tianjin 300071, People's Republic of China, and [⊥]Display Laboratory, Materials and Device Institute, Samsung Advanced Institute of Technology, Samsung Electronics CO., LTD., Yongin, 446-712, Korea

ABSTRACT Reduced graphene oxide (RGO) is an electrically conductive carbon-based nanomaterial that has recently attracted attention as a potential electrode for organic electronics. Here we evaluate several solution-based methods for fabricating RGO bottom-contact (BC) electrodes for organic thin-film transistors (OTFTs), demonstrate functional p- and n-channel devices with such electrodes, and compare their electrical performance with analogous devices containing gold electrodes. We show that the morphology of organic semiconductor films deposited on RGO electrodes is similar to that observed in the channel region of the devices and that devices fabricated with RGO electrodes have lower contact resistances compared to those fabricated with gold contacts. Although the conductivity of RGO is poor compared to that of gold, RGO is still an enticing electrode material for organic electronic devices possibly owing to the retention of desirable morphological features, lower contact resistance, lower cost, and solution processability.

KEYWORDS: reduced graphene oxide · organic semiconductors · OTFT · compatible interfaces · thin-film morphology · contact resistance

Organic thin-film field-effect transistors (OTFTs) switch and modulate current using a thin-film of an organic compound as the active electronic material.[1,2] This organic component makes them attractive in a range of high-value applications that are complementary to those of silicon-based electronics.[3−5] Such applications involve situations requiring low weight, flexibility, transparency, conformal coverage of nonplanar and complex surfaces, large format, low cost per area, chemical and biological sensing, *etc.*[6−9] Many factors can intervene to shape the end performance of OTFTs including the purity of the organic semiconductor, the thin-film processing, the choice of gate dielectrics and of electrical contacts, *etc.*[5,10−12] The richness of such phase-space makes OTFT research both challenging and exciting as the foreseen applications come closer to reality. In this work we focus on the fabrication and performance of graphene-oxide-based electrical contacts for OTFTs.

Reduced graphene oxide (RGO) comprises a class of nanometer-scale materials resulting from the sequential oxidation and reduction of graphene.[13,14] Graphene is a two-dimensional semimetallic nanocarbon allotrope with physical properties relevant to applications from mechanical reinforcement to transparent electrical conductors and the study of quantum phenomena.[14−17] Graphene is difficult to process on a large scale since the material is insoluble and does not sublime. Thermal desorption of Si from SiC[15,18] and, recently, vapor-deposition methods[19,20] are common approaches to fabrication of graphene films. In contrast, graphene oxide (GO) can be deposited from water suspensions,[13,21] and solution-processed GO has been used to form stand-alone films,[22] prepare composites[15,16] and obtain large-scale films.[23,24] Importantly, GO films are electrically insulating[25,26] but can be reduced through chemical reduction,[27] hydrogen plasma,[28] or thermal desorption of oxygen content to yield RGO.[25] RGO is graphene-like, yet it has an imperfect lattice due to loss of carbon during reduction, residual oxygenated sites, residual sp^3-hybridized cycloalkane domains, and the physical grain boundaries between the original GO sheets.[21,26] Such defects can reduce conductivity and charge carrier mobility,[14] yet RGO has been found useful as a conductor for transistor[29] and photovoltaic applications.[30,31] Projected advantages of

*Address correspondence to zbao@stanford.edu.

Received for review January 22, 2010 and accepted October 04, 2010.

Published online October 14, 2010.
10.1021/nn101369j

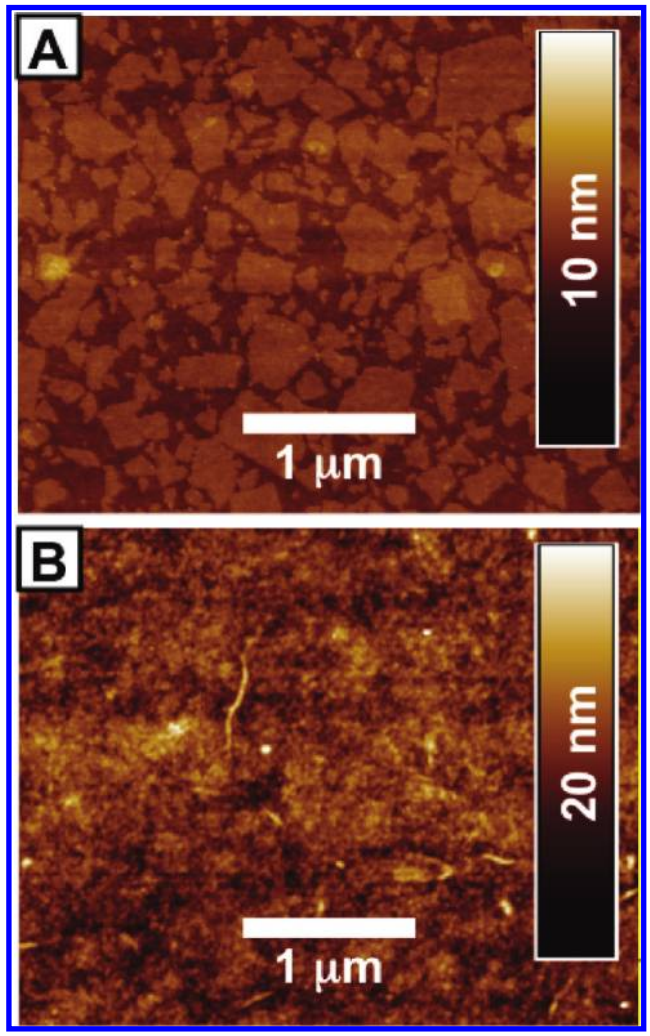

Figure 1. Tapping-mode AFM height images of spin-coated GO deposited on Si/SiO_2 substrates: (A) sum-monolayer coverage, individual GO sheets, with approximate lateral dimensions on the order of 200−400 nm; (B) multilayer, fully connected, ~20 nm GO film.

using RGO in these devices compared to traditional materials include high material abundance, high material stability, lower material cost, simpler and less costly processing, and suitability for large area applications.

Previous work in the community has demonstrated the use of graphene-like electrodes for OTFTs. For example, Liu's group utilized a patterned metal catalyst film to grow few-layer graphene electrodes using a high-temperature (≈ 800 °C) vapor−liquid−solid method[20] and demonstrated good performance in pentacene OTFTs despite of the high roughness of their electrodes. In another example, Müllen's group reported the patterning of solution-deposited RGO films using oxygen plasma to delineate RGO electrodes and further demonstrated low-contact resistance of these electrodes in pentacene OTFTs.[29] Our work complements these previous reports because we (1) propose several, easily accessible electrode fabrication methods, (2) explore the effects of the fabrication process on the RGO electrode efficiency, (3) demonstrate charge injection into p- and n-channel materials, (4) corroborate the finding of lowered contact resistance compared to gold electrodes, and (5) highlight the need to explore the effect that RGO electrodes have on the growth of organic semiconductor thin-films.

For this study we selected three different organic semiconductors as the active OTFT material: pentacene (p-channel),[32] copper(II) hexadecafluorophthalocyanine (F_{16}CuPc) (n-channel),[33] and poly(didodecylquaterthiophene-alt-didode-cylbithiazole) (PQTBTz-C_{12}) (p-channel).[34] The chemical structures of these materials are shown in Figure S1 in the Supporting Information. Thin-films of these materials were deposited onto our RGO electrodes to form BC OTFTs as detailed in the OTFT fabrication and methods sections.

RESULTS AND DISCUSSION

Preparation and Characterization of RGO Films. All water used was 18 MΩ grade. RGO films were spin-coated from aqueous suspensions of GO on cleaned substrates followed by reduction of the GO to obtain RGO. The GO powder was prepared as described previously and in the methods section.[25] Figure 1A is an atomic force microscopy (AFM) image displaying individual GO sheets in a submonolayer film; Figure 1B depicts a typical multilayer film, ~20 nm thick. Several reductive treatments for GO films were investigated as described in Table S1 in the Supporting Information. We selected a reductive treatment consisting of a 3 h thermal annealing at 400 °C in an argon environment because it provided a suitable compromise between process cost, applicability, electrical conductivity, and electrode work function. The resulting RGO material had a typical thickness of ~15 nm, a work function of 5.01 eV, and a four-point probe conductivity of 71 S cm^{-1}.

Methodologies for RGO Electrode Patterning. We investigated three different methods of increasing complexity for patterning RGO electrodes in order to determine the best method for patterning RGO for OTFTs. These methods are depicted in Schemes 1−3.

Method 1 is the reduce-pattern (R-P) process and it follows the black line in Scheme 1: (1) spin-coat a GO film on a transistor substrate; (2) reduce the film; (3) pattern the RGO film using oxygen plasma and a metal shadow mask. This approach is a simplification of that

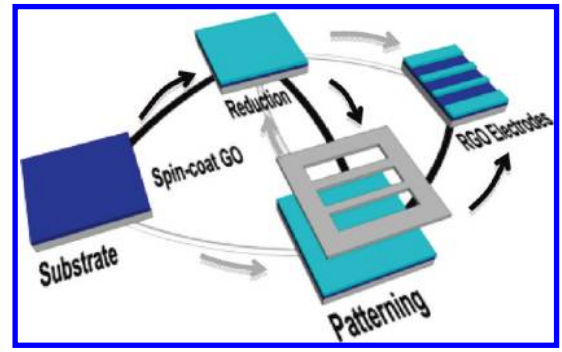

Scheme 1. R-P (black path) and P-R (gray path) fabrication of RGO electrodes on plain SiO_2/Si transistor substrates.

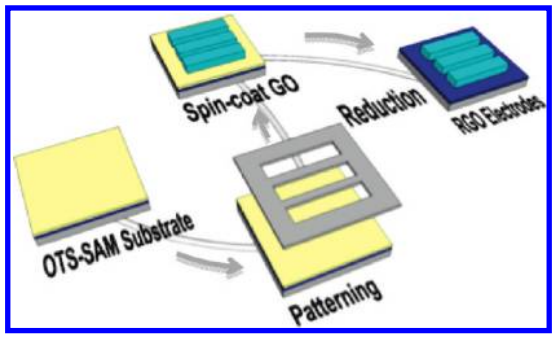

Scheme 2. SAM sacrificial layer method for RGO electrode patterning.

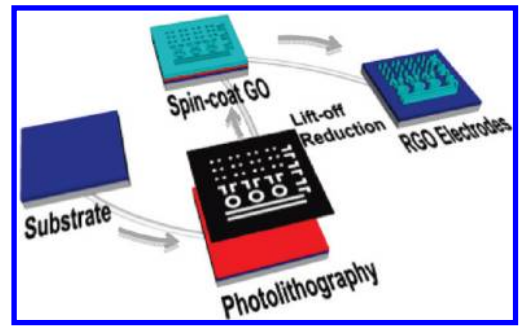

Scheme 3. Photolithography method for RGO electrodes.

reported by Müllen's group,[29] and differs from it in two main respects: (i) reusable metal shadow mask replaces the single-use sacrificial Al layer; (ii) the RGO pattern obtained is the negative of the shadow mask, so all RGO features are "shorted" and a method for "disconnecting" them is required. For example, we achieved isolated devices by scoring the RGO film or by cleaving the substrate. This characteristic might restrict the RGO patterns to relatively large and geometrically simple features, but it does not require access to a metal evaporator, so the R-P process may be useful in some settings. OTFT devices fabricated on R-P electrodes showed poor performance, likely due to oxidation of the electrode edges during patterning. Reversing the order of the reduction and patterning (a P-R process that follows the gray line in Scheme 1), greatly improved the electrode performance in OTFT devices because the reduction step reverses the effects of the oxygen plasma on the RGO. We used scanning-electron microscopy (SEM) coupled with Auger electron spectroscopy (AES) to probe the composition of the edges of our R-P and P-R RGO electrodes and found that R-P electrodes indeed show highly oxidized edges compared to P-R electrodes. This analysis is shown in Figure S2 in the Supporting Information.

Fabrication method 2 eliminates the image-reversal observed in method 1 by using a high quality self-assembled monolayer (SAM) of octadecyltrimethoxysilane (OTS) as a sacrificial layer.[35] Scheme 2 shows the process flow: a transistor substrate bearing an OTS SAM (contact angle $\approx$ 106°) is exposed to O_2 plasma through a metal shadow mask, and a GO suspension is spin-coated on the substrate. GO selectively deposits on the freshly etched, hydrophilic patterns and dewets from the hydrophobic OTS regions of the substrate. Next, the RGO film is thermally reduced as described above to complete the electrode fabrication. Devices bearing these RGO electrodes show improved charge injection at the electrode-semiconductor interface because the RGO was never exposed to O_2 plasma. A potential disadvantage of this method is the limited resolution of the wetting/dewetting patterning. We have so far demonstrated features in the order of $\sim$500 μm and further optimization might push the limit to $\sim$100 μm. Additional improvements in resolution might require solution-processing methods other than spin-coating, such as solution-shearing,[12] vortex deposition,[36] or jet-printing.[37] Importantly, limited spatial resolution might not be a significant deterrent in large area applications, where solution-processed RGO electrodes would likely be used.

Method 3 eliminates the resolution and feature complexity limitations of the previous methods by using photolithographic processing as shown in Scheme 3. A transistor substrate is coated with a thin-photoresist layer and the electrode pattern is transferred to it using conventional photolithography. After development, the GO dispersion is spin-coated on the substrate followed by a soft bake to fix GO to the developed regions. Unexposed photoresist and the GO that covers it are lifted-off using a solvent bath. Next, the patterned GO features undergo thermal reduction to yield finished RGO electrodes. Figure 2 shows microscopic characterization of these electrodes. To date, we have demonstrated well-resolved electrode gaps as narrow as 2 μm with this fabrication technique.

OTFT Fabrication and Influence of Electrode Material on Organic Semiconductor Morphology. To study the influence of RGO on semiconductor morphology, we prepared large area OTS-modified substrates, unpatterned RGO substrates and substrates bearing 40 nm of evaporated gold. Next we cleaved each large substrate in two pieces and evaporated a 40 nm film of pentacene onto one set of fragments and 40 nm of F_{16}CuPc onto the other. We examined the differences in film morphology using X-ray diffraction (XRD) and AFM, and the results are summarized in Figures 3 and 4. Figure 3A shows XRD spectra from pentacene films deposited on gold, OTS, and RGO substrates. Pentacene deposited on OTS-treated substrates is highly crystalline, and the d(001) spacing found (16.06 Å) corresponds well to that reported in the literature (15.4 Å),[38−40] indicating that the pentacene molecules deposit edge-on on this surface. Pentacene evaporated onto RGO retains the first two peaks, although with much reduced intensity, indicating that the ordering of the film is less significant, possibly because of surface roughness of the RGO and because of interactions between the π-electrons of RGO and pentacene that might cause some molecules

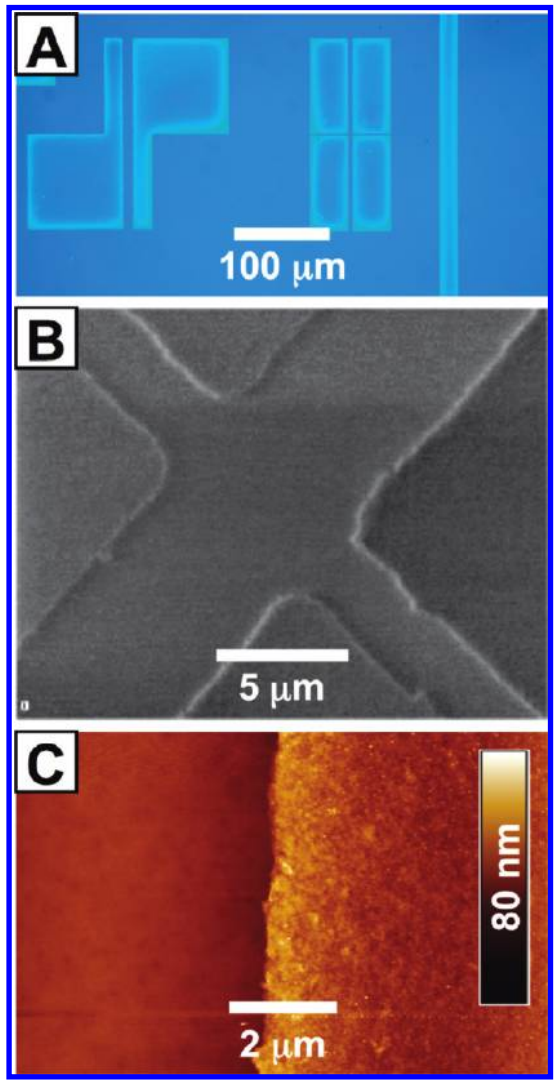

Figure 2. Photolithographically patterned RGO electrodes. (A) Bright-field optical micrograph showing RGO electrodes of various sizes: the gaps are 10, 5, and 2 μm; the width of the electrodes is always 20× the gap size, to give a constant W/L of 20. (B) SEM image showing well-defined 5 μm and a 2 μm electrode gap. (C) Tapping-mode AFM height image of the edge of a photopatterned RGO electrode showing a well-defined edge with no residual photoresist.

to tilt. As expected, pentacene deposited on gold-coated substrates does not contain any of the characteristic peaks of the reported phases, since it is well-known that pentacene deposited on gold grows in a highly disordered three-dimensional phase.[2,40,41] Figure 3B contains corresponding XRD data for F_{16}CuPc films, displaying the same general trend as for pentacene. F_{16}CuPc on OTS presents two small peaks, and the film on RGO clearly retains the first peak, but F_{16}CuPc on gold does not show any of these peaks likely for similar reasons as discussed for pentacene. These findings suggest that RGO films are more compatible with 2D-growth of semiconductor than gold surfaces and the differences between growth on OTS (contact angle ≈ 106°) and RGO (contact angle ≈ 73°) are likely due to

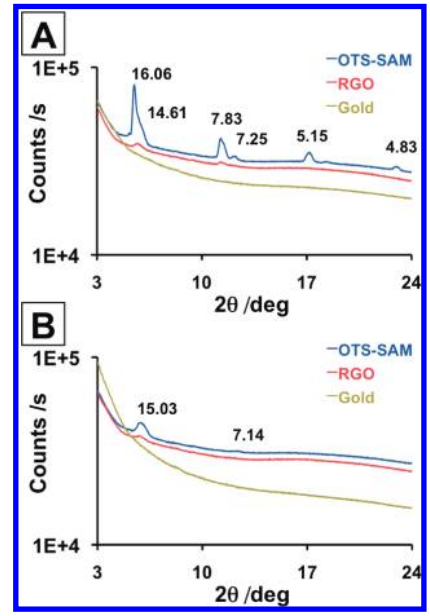

Figure 3. XRD characterization of (A) pentacene and (B) F_{16}CuPc films evaporated on different substrate materials. Semiconductor films on RGO samples retain some of the morphology displayed on OTS-treated surfaces, while films on gold are completely different.

differences in surface roughness, hydrogen content, and surface energy.

Figure 4 summarizes an AFM study of the morphology of pentacene deposited concurrently on OTS, RGO, and gold surfaces to a nominal film thickness of 42 nm. Pentacene on OTS-treated surfaces displayed the expected terraced structure of two-dimensional pentacene plates (Figure 4A). Figure 4B shows the less-ordered, but still two-dimensional (note *Z* scale) morphology of pentacene deposited on RGO surfaces. In contrast, Figure 4C displays the well-known three-dimensional morphology of pentacene films deposited on gold. These images strongly suggest that films in Figure 4A,B might form better interfaces with contacts than the film in Figure 4C, thus facilitating charge injection into the semiconductor. Figure 4D shows the actual transition region from pentacene deposited on an RGO electrode to pentacene deposited on the OTS-treated active channel. While the morphologies are not identical, pentacene grows two-dimensionally on both surfaces facilitating efficient charge transfer from the semiconductor atop the RGO electrode to the semiconductor deposited on the active channel of the OTFT.[40,41] Such differences might be relevant when considering the different contact resistances measured in OTFTs bearing RGO and gold electrodes since the morphological changes of the pentacene film from electrode to channel are much more drastic in the latter case.

Comparison of Transistor Performance of OTFTs with RGO or Gold Electrodes. We fabricated OTFTs bearing RGO electrodes from each of the three methods discussed above. Devices with R-P electrodes performed poorly, but all other devices showed comparable performance

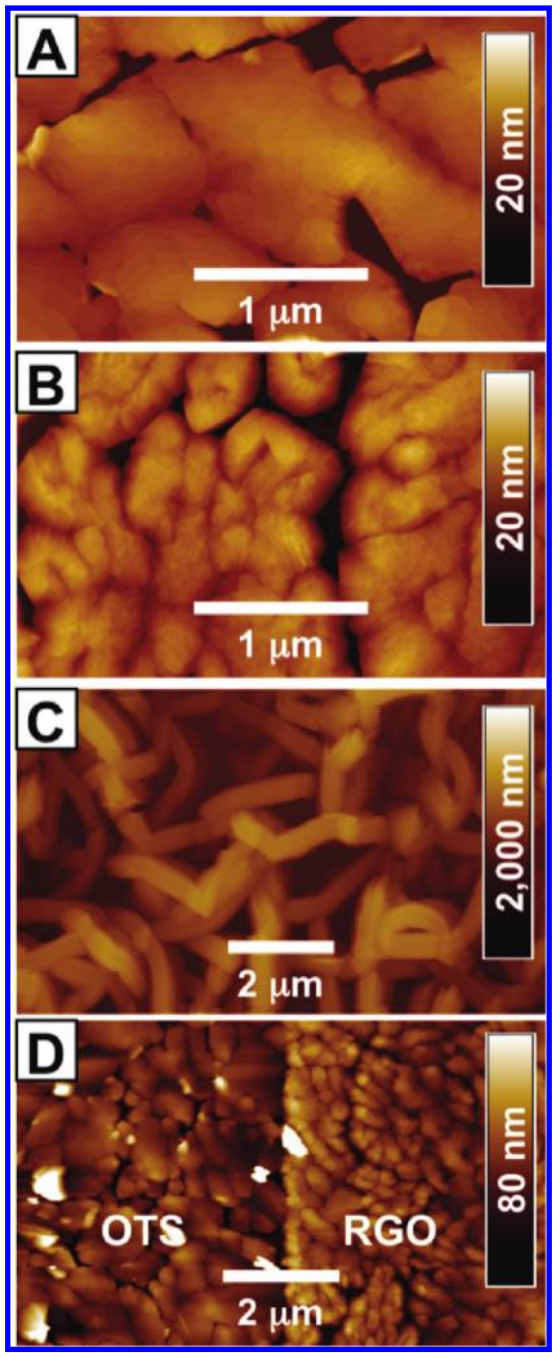

Figure 4. AFM tapping-mode height images of pentacene films deposited during the same evaporation experiment on (A) OTS-treated, (B) RGO, and (C) gold-coated surfaces. (D) AFM image of pentacene at the interface between RGO and OTS. The nominal pentacene film-thickness was 42 nm and the *Z*-scales of (A) and (B) were adjusted to allow appreciation of the surface detail at the expense of detail at the bottom of the films. Note that the *Z*-scale in (C) has to be 100 times greater to show the top surface of this rough film.

because patterned RGO is identical after the reduction step. The analysis below focuses on OTFTs fabricated using photolithographically patterned RGO because the length and width of the active channel can be precisely controlled with this fabrication method.

Figure 5 shows a transfer-line method (TLM)[42−44]

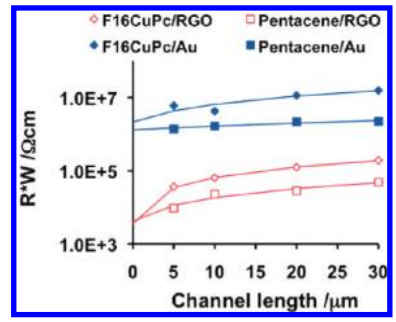

Figure 5. TLM-estimated, width-normalized contact resistance between RGO or gold electrodes and pentacene or F_{16}CuPc. *Y*-axis scale is logarithmic to display the RGO and gold values in one figure. Fits shown are straight lines when plotted on a linear scale. *W*/*L* = 20 and *L* varies as indicated in the *X*-axis.

plot that was used to estimate the contact resistances of pentacene/RGO and F_{16}CuPc/RGO, pentacene/gold, and F_{16}CuPc/gold devices. The aspect ratio of the active OTFT channel (width of the channel divided by its length, *W*/*L*), was kept constant at a value of 20 for all devices. We found that our estimated contact resistance for BC pentacene/gold OTFTs ($\sim 1 \times 10^6\ \Omega$ cm) correlates well with literature values, which vary in the range 4×10^4 to $7 \times 10^6\ \Omega$ cm depending on the semiconductor film thickness and deposition conditions.[42,45] RGO electrodes show ~100× lower contact resistance for charge injection into the selected organic semiconductors than gold electrodes (SAM-modified gold electrodes have lower contact resistances because of their different surface dipoles and energies).[10,46] This finding may, at first, seem counterintuitive since the resistance of the RGO electrode itself is $\sim 6 \times 10^3$ times higher than that of gold (Table S1 in Supporting Information). However, the parameter being evaluated is not the transfer of charge carriers through the electrode, but the transfer of charge carriers across the electrode/semiconductor interface and across the organic semiconductor transitioning from the electrode into the channel region of the OTFT. Higher contact resistances can be expected between organic semiconductors and metals due to the interface dipole barrier that forms when π-electrons from conjugated molecules adsorb on metal surfaces. These electrons push back electron density from the metal surface and can effectively lower the surface-dipole contribution to the metal work function by as much as 0.5−1.0 eV. Interorganic systems, such as our RGO/organic semiconductor, are not as susceptible to these effects since RGO has significantly lower surface electron density compared to a metal, resulting in RGO's workfunction having only a small surface dipole contribution to it.[47] Other carbon-containing materials have also been shown to have lower contact resistance than gold for charge injection into organic semiconductor materials.[29,48] A common feature in all these observations is that the carbon-based electrode is electron donating and the organic semiconductor is electron-accepting relative the elec-

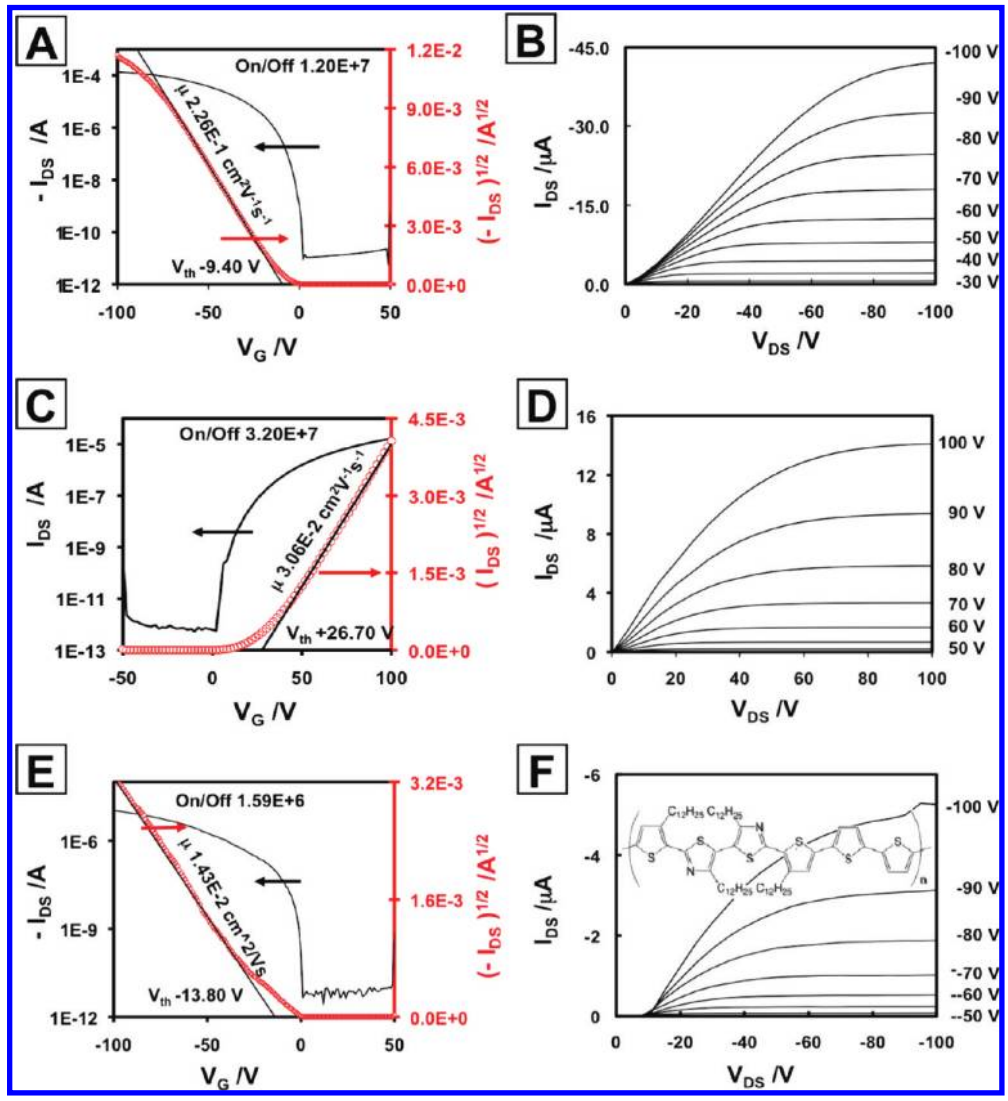

Figure 6. *I*−*V* relations for OTFT devices with RGO electrodes. Panels A, C, and E are transfer curves for pentacene, F_{16}CuPc, and PQTBTz-C_{12}, respectively. V_{DS} was −100 V in all cases. Panels B, D, and F are output series for pentacene, F_{16}CuPc, and PQTBTz-C_{12}, respectively, with the structure of the polymer shown as an overlay in panel F. The channel aspect ratio *W*/*L* is 20 in all cases, and *L* is 30 μm.

trode. Such interorganic interfaces have been shown to have enhanced charge transport.[49] Beyond electronic effects, our film morphology studies suggest that unlike gold, RGO allows the formation of smooth 2D-grains at the electrode/semiconductor interface, likely yielding improved connectivity with grains growing at the OTS-treated active channel and facilitating better charge transfer into the channel. Thus the lowered contact resistance we observe might have various contributing factors that will need to be elucidated and optimized elsewhere. In the future, other factors that could lead to further reductions in contact resistance include controlling the crystallinity and morphology of the semiconductor film,[10,46] performing postreductive treatment of the RGO surface with appropriate SAMS,[46,47] and doping the RGO material.

Next we characterized the electronic performance of OTFTs bearing photolithographically patterned RGO electrodes. Figure 6 panels A, C, and E display the transfer curve characteristic, or the plot of drain-source current (I_{DS}) *vs* gate voltage (V_G), for OTFTs where the active layer is a film of (A) pentacene, (C) F_{16}CuPc, and (E) PQTBTz-C_{12}, respectively. In each case the curve is well behaved, has a clear on−off transition, an I_{ON}/I_{OFF} ratio $> 10^6$, and a reasonably low threshold voltage (V_{th}) for BC devices on 300 nm silicon dioxide dielectrics. The field-effect mobilities (FET-μ) extracted from the *I*−*V* curves of our nonoptimized devices are 2.26×10^{-1} for pentacene, 3.06×10^{-2} for F_{16}CuPc, and 1.43×10^{-2} cm^2 V^{-1} s^{-1} for PQTBTz-C_{12}. The mobilities for pentacene and F_{16}CuPc OTFTs are of the same order of magnitude as those reported in the literature (*ca.* 5×10^{-1} and *ca.* 3×10^{-2} cm^2 V^{-1} s^{-1} for BC pentacene[42] and F_{16}CuPc[33] OTFTs, respectively). Our BC PQTBTz-C_{12}/RGO devices showed significantly lower FET-μ than the recently reported top-contact PQTBTz-C_{12}/gold (3.3×10^{-1} cm^2 V^{-1} s^{-1}),[34] yet, top-contact OTFTs typically show improved performance over BC devices due in

TABLE 1. Comparative Transistor Performance of RGO and Gold-Based OTFT Devices

material	contact	I_{DS}[a]	av FET-μ[b]	max FET-μ[c]	V_{th}[d]	I_{ON}/I_{OFF}[e]
pentacene	RGO	$1.19 \times 10^{-4} \pm 9\%$	$1.80 \times 10^{-1} \pm 14\%$	2.11×10^{-1}	-7.0 ± 0.6	5.23×10^{6}
	gold	$9.95 \times 10^{-6} \pm 9\%$	$1.05 \times 10^{-2} \pm 0.2\%$	1.05×10^{-2}	-1.9 ± 3.8	5.75×10^{5}
F_{16}CuPc	RGO	$1.60 \times 10^{-5} \pm 26\%$	$2.76 \times 10^{-2} \pm 23\%$	3.30×10^{-2}	26.1 ± 3.4	1.00×10^{7}
	gold	$4.41 \times 10^{-7} \pm 17\%$	$1.10 \times 10^{-3} \pm 25\%$	1.38×10^{-3}	38.7 ± 1.0	6.23×10^{5}
PQTBTz-C_{12}	RGO	$6.34 \times 10^{-6} \pm 75\%$	$8.96 \times 10^{-3} \pm 77\%$	1.47×10^{-2}	-11.1 ± 9.9	1.04×10^{6}
	gold	$4.65 \times 10^{-7} \pm 13\%$	$1.07 \times 10^{-3} \pm 15\%$	1.20×10^{-3}	-24.7 ± 8.4	3.54×10^{4}

[a]Average drain-source current at the end maximum of the transfer curve, given in amps, dispersion indicated as a relative standard deviation (RSD). [b]Average field-effect mobility given in $cm^2 V^{-1} s^{-1}$. [c]Maximum field-effect mobility measured on that material, given in $cm^2 V^{-1} s^{-1}$. [d]Average threshold voltage of OTFT operation, given in volts. [e]Average ratio of the I_{DS} currents in the ON and in the OFF state.

part to film-morphology considerations.[1,41] As will be shown below, our BC PQTBTz-C_{12}/RGO devices did achieve higher FET-μ than corresponding BC PQTBTz-C_{12}/gold controls. These observed improvements in OTFT performance are likely due at least in part to the influence of RGO electrodes on the morphology of the semiconductor thin-film, which might facilitate charge injection. A recent report[50] describing the use of RGO as a gold-modification layer in BC pentacene OTFTs also concurs that RGO improves charge injection into pentacene, achieving a maximum FET-μ of 1.3×10^{-1} cm^2 V^{-1} s^{-1}. The benefit of the higher mobilities achieved using RGO electrodes may be counterbalanced with the operational issues that arise from the high resistivity of RGO itself. Thus, under continued operation, devices bearing RGO electrodes are likely to experience local heating at the electrode/semiconductor interface, which could, depending on the temperatures reached, physically or chemically accelerate the degradation of the organic semiconductor layer. While such a scenario might not be too worrisome for proof-of-concept devices and circuits, the issue of high RGO resistivity should be resolved either by doping or by improved preparative methods before the material is truly useful in large-format, heavy use applications.

Figure 6 panels B, D, and F display the output curve series, or the plot of I_{DS} *vs* drain-source voltage (V_{DS}), measured at incremental V_G values for pentacene, F_{16}CuPc, and PQTBTz-C_{12} on RGO electrodes, respectively. Generally speaking these measurements provide more information regarding the physics of the devices than the corresponding transfer curves. As such we can see the pentacene curves (Figure 6B) have a sublinear onset, with the bending of the curves becoming more noticeable as the magnitude of V_G increases. In spite of this feature, the curves achieve excellent saturation behavior, although the current scaling between curves is not fully quadratic. The F_{16}CuPc curves in Figure 6D show linear onsets with well-developed saturation regions for all V_G traces. The scaling increases more rapidly than pentacene OTFTs, although it is still not quadratic. To a first approximation the energetics for charge injection alone do not explain why the pentacene has charge injection difficulties since the level of its highest occupied molecular orbital (HOMO) is reported at 4.96 eV,[51] significantly closer to the RGO workfunction (5.01 eV) than the lowest unoccupied molecular orbital (LUMO) of the F_{16}CuPc, reported at 4.80 eV.[52] Importantly, literature reported values often capture the conditions at the top surface of the semiconductor films, while additional factors such as interface polarization[53] and local orientation effects of semiconductor molecules at the contact surface need to be considered to rationalize charge injection barriers in the actual devices.[54,55] Despite the lower contact resistance than gold-BC devices, our RGO devices still show significant contact resistance at low drain−source voltages. Finally, Figure 6F shows the curves for the conjugated polymer. In this case we see a complete shift of the curves to higher V_{DS} values indicating a significant contact resistance that must be overcome before current can efficiently flow through the device. The output traces do reach saturation and seem to show good scaling, yet the inferior quality of this device is clear from the onset shift and in the instability of the high V_G trace. We propose that the relatively poor performance of these polymer devices may be partially due to the nonoptimized solution-processing involved in their fabrication.

Finally, Table 1 compares key performance parameters for RGO-based and gold-based OTFTs for each of the three semiconductors. In every case, currents, mobilities, and I_{ON}/I_{OFF} ratios are higher for the RGO-electrode devices than for the gold electrode devices, once again suggesting that charge injection is more efficient at the RGO/organic semiconductor interface. Furthermore we observe that the performance enhancement is slightly higher for small molecules than for the polymer which might be correlated with film morphology effects at the RGO electrodes. For example, average FET-μ is at least a factor of ~17× higher in RGO than in gold for pentacene and F_{16}CuPc, while it is only a factor of ~9× higher in RGO for the conjugated polymer. This may be related to the greater ease with which small organic semiconductor molecules form ordered domains in the solid state compared to the larger mol-

ecules of the conjugated polymer which tend to form amorphous films and can be less sensitive to the electrode surface.

CONCLUSIONS

We demonstrated a versatile approach for the fabrication of RGO electrodes including solution processing of unreduced GO and patterning of the same using oxygen plasma or photolithography. We evaluated several reductive methods to form RGO from GO and studied their effect on the properties of RGO as an electrode material. We also characterized the effect of the RGO surface on the morphology of overlaying organic thin-films. Functional p- and n-channel OTFT with RGO electrodes were fabricated using small-molecule and polymer semiconductors. Bottom contact devices with RGO electrodes displayed lower contact resistance and higher mobilities than similar OTFTs with gold electrodes. Future research directions may include the detailed study of molecular orientation at the RGO interface, determination of the magnitude and effect of surface RGO dipoles, functionalization and doping of RGO electrodes to increase their conductivity and to further improve charge injection, and comparison of the performance of RGO electrodes with Al or Mo electrodes for n-channel materials. Importantly, our current findings suggest that notwithstanding their high electrical resistance compared to gold, RGO electrodes may be suitable for the fabrication of large area organic electronic devices owing to the abundance and relatively low cost of the starting material, their facile and relatively low-cost processing, and the possibility for nanometer-scale functionalization and control of individual GO sheets.

METHODS

Preparation of Water-Soluble Graphene Oxide Powder. Graphene oxide was prepared using modified Hummers method[56] from flake graphite (average particle diameter of 4 μm, 99.95% purity, Qingdao Tianhe Graphite Co. Ltd., Qingdao, China). Briefly, 5 g of graphite and 3.75 g of $NaNO_3$ as received (A.R.) were placed in a flask. Then, 375 mL of H_2SO_4 (A.R.) was added with stirring in an ice−water bath, and 22.5 g of $KMnO_4$ (A.R.) were slowly added over about 1 h. Stirring was continued for 2 h in the ice−water bath. After the mixture was stirred vigorously for 5 days at room temperature, 700 mL of 5 wt % H_2SO_4 aqueous solution was added over about 1 h with stirring, and the temperature was kept at 98 °C. The resultant mixture was further stirred for 2 h at 98 °C. The temperature was reduced to 60 °C, 15 mL of H_2O_2 (30 wt % aqueous solution) was added, and the mixture was stirred for 2 h at room temperature. Next, ions of oxidant and other inorganic impurity were removed repeating the following procedure cycle 15 times: centrifugation, removal of the supernatant liquid, addition of 2 L of a mixed aqueous solution of 3 wt % H_2SO_4/0.5 wt % H_2O_2 to the bottom solid, and dispersion of the solid using vigorous stirring and bath ultrasonication for 30 min at a power of 140 W. Then a similar procedure was repeated three times using 3 wt % HCl aqueous solution (2 L) and one time using H_2O (2 L). The resultant water solution was passed through a weak basic ion-exchange resin (D301T, Nankai University Chemical Plant) with water as mobile phase to remove the remaining HCl. Then water was removed through a drying process for the collected solution to yield 3.5 g of product.

Substrate Preparation and Deposition of GO Films. For basic transistor substrates we used highly doped n-type (100) Si wafers (<0.004 Ω cm)with a 300 nmdry thermal oxide gate dielectric (capacitance C_i = 10 nF cm^{-2}) and cleaned them in piranha solution (7:3 H_2SO_4/H_2O_2 mixture, CAUTION: extremely corrosive and highly exothermic) for 40 min followed by extensive rinsing with deionized water and storage under water until the moment of RGO deposition. For OTS-SAM sacrifical layer substrates, a 0.1% solution of octadecyl- trimethoxysilane (Gelest Inc., Morrisville, PA) in trichloroethylene (EMD Chemicals Inc., Darmstadt, Germany) was spin-coated on the cleaned wafers and allowed to react overnight at room temperature in the presence of ammonia vapor. Excess silane was removed by ultrasonication in toluene, followed by rinsing with toluene, acetone and isopropyl alcohol, and drying under a stream of nitrogen. OTS-treated wafers typically showed a contact angle of approximately 105°. Patterned photoresist substrates were prepared in a cleanroom using standard photolithography techniques. The patterned and developed photoresist-coated transistor substrates were then kept in sealed containers and subjected to a brief, 20 s oxygen plasma treatment (200 W, 150 mTorr O_2) to activate the exposed silicon dioxide surfaces. Etching of RGO for fabrication of P-R and R-P electrodes was performed by exposure to oxygen plasma with slightly harsher conditions: 200 W, 200 mTorr O_2, and 120 s.

GO was deposited on freshly cleaned basic transistor substrates or on freshly patterned OTS-SAM substrates by spin-coating. First, these substrates were dried using high spin rates. Then a volume of aqueous GO dispersion (~3 mg/mL) sufficient to cover the whole substrate was allowed to rest on the substrate for 15 s, after which the spin-rate was increased from 0 to 1200 rpm in a linear fashion over 60 s. Films were dried by placing them on a hot plate at 110 °C for 30 min before any reducing treatments. Deposition of GO films on photoresist-coated differed in that the films were dried for 1 min at 110 °C before a lift-off step in warm acetone, after which the films were dried again on a hot plate at 110 °C for 30 min.

GO Reduction Treatments. ***Hydrazine Vapor Reduction.*** GO films on substrates were placed in a clean glass Petri dish nested in a larger glass Petri dish which also contained 1 mL of hydrazine monohydrate 98% (Alfa Aesar, Ward Hill, MA). The larger dish was covered with a glass lid, sealed with Parafilm tape, and placed over a hot plate at 40 °C for 18 h, after which the dish was opened and the films were rinsed with purified water and dried both under a nitrogen stream and by heating to 80 °C in vacuum. GO films changed color after the hydrazine vapor treatment, from matte brown to metallic gray, indicating reduction of the material.

Thermal Annealing at 400 °C under Argon Flow. Dry GO films on substrates were loaded inside a 2 cm internal diameter cylindrical quartz boat with open ends. The boat was introduced in a 1 in. internal diameter glass tube oven fitted with controlled vacuum and gas flow. Films were heated under a continuous flow of 70 standard cubic centimeters of ultrapure argon, at a rate of 20 °C/min, held at 400 °C for 3 h, and allowed to cool to room temperature over 1 h.

Graphitization in Vacuum at 1100 °C. Dry GO films on substrates were placed in quartz boats inside a 3 ft long 1 in. diameter quartz tube with one end closed. The tube was introduced into a Lindberg/BlueM split hinge oven (Lindberg/Blue M 3-zone tube oven, Blue-M, White Deer, PA) and the open end was fitted to a turbopump vacuum line (Turbo-V 250 MacroTorr, Varian Inc., Palo Alto, CA). Films were heated to 100 °C at ambient pressure, then the turbo pump was switched on and a vacuum of 10^{-5} Torr was established before heating to 1100 °C. Heating rates as high as 20 °C/min could be achieved without loss of films. The temperature was held constant at 1100 °C for 3 h after which the system was allowed to cool down (3 h).

Deposition of Organic Semiconductor Materials. Small molecule organic semiconductors were simultaneously deposited onto RGO, OTS-SAM and gold surfaces using an Angstrom thermal evapo-

rator and a rotating substrate holder. Base-pressure for our depositions was 3×10^{-6} Torr. Triply sublimed pentacene (Aldrich) was deposited at a rate of ~0.5 Å s^{-1}, with a substrate temperature of 60 °C, and film thickness was ~40 nm. F_{16}CuPc (Aldrich) was used as received and was also deposited onto a room temperature substrate at a rate of ~0.5 Å s^{-1}, and film thickness was ~50 nm. PQTBTz-C_{12} was spin-coated onto RGO or gold electrode substrates by spin-coating from a 3 mg/mL solution in anhydrous chlorobenzene (Sigma-Aldrich). These polymer films were dried by heating them for 3 h inside a vacuum oven at 80 °C and were subsequently annealed by heating to 180 °C for 1 h in a dry N_2 environment followed by slow cooling to room temperature.

OTFT Measurements. The OTFT transfer and output characteristics were recorded in air using a Keithley 4200 semiconductor parametric analyzer (Keithley Instruments, Cleveland, OH).

Characterization of Film Topography and Composition. Tapping-mode AFM investigation of the films was accomplised using a Multimode Nanoscope III with Extender electronics (Digital Instruments/Veeco Metrology Group, Santa Barbara, CA). Film thickness measurements were performed with a Dektak 150 profilometer (Veeco Metrology Group). Auger electron spectra (AES) were collected with a PHI 700 Scanning Auger Nanoprobe (Physical Electronics, Inc.) equipped with secondary electron imaging and 10 nm Auger resolution with high elemental sensitivity. XRD analysis was completed as follows: We deposited 40 nm pentacene and 50 nm F_{16}CuPc films on sets of freshly prepared RGO, OTS-SAM, and gold-coated substrates. These films were analyzed using a Philips PANalytical X'Pert diffractometer using the Cu Kα line. Work function measurements were performed on large area thin-films of the material of interest supported on silicon dioxide substrates using a Riken Keiki PES system model AC-2.

Acknowledgment. We thank Colin C. Reese for access to and training in the use of the glass-tube furnace with controlled argon flow. M.L.T. acknowledges a Kodak graduate fellowship. M.R. acknowledges partial support from NASA GSRP. Z. Bao acknowledges partial financial support from the Samsung Advanced Institute of Technology and from a Sloan Research Fellowship. We thank the Center for Polymeric Interfaces and Macromolecular Assemblies (NSF-Center MRSEC under Award Number DMR-0213618) for the use of shared facilities. Y. Chen gratefully acknowledges the financial support from MoST (#2006CB0N0702), MoE (#20040055020), and the NSF (#20774047 and 60676051) of China.

Supporting Information Available: Materials used in this study; characterization of GO reduction methods and electrode edges. This material is available free of charge *via* the Internet at http://pubs.acs.org.

REFERENCES AND NOTES

1. Horowitz, G. Organic Thin Film Transistors: From Theory to Real Devices. *J. Mater. Res.* **2004**, *19*, 1946–1962.
2. Dimitrakopoulos, C. D.; Malenfant, P. R. L. Organic Thin Film Transistors For Large Area Electronics. *Adv. Mater.* **2002**, *14*, 99–117.
3. Bao, Z. *Organic Field-Effect Transistors*; Bao, Z., Locklin, J., Eds.; CRC-Press: Boca Raton, FL, 2007.
4. Forrest, S. R.; Thompson, M. E. Introduction: Organic Electronics and Optoelectronics. *Chem. Rev.* **2007**, *107*, 923–925.
5. Sirringhaus, H.; Ando, M. Materials Challenges and Applications of Solution-Processed Organic Field-Effect Transistors. *MRS Bull.* **2008**, *33*, 676–682.
6. Dodabalapur, A. Organic and Polymer Transistors for Electronics. *Mater. Today* **2006**, *9*, 24–30.
7. Sekitani, T.; Nakajima, H.; Maeda, H.; Fukushima, T.; Aida, T.; Hata, K.; Someya, T. Stretchable Active-Matrix Organic Light-Emitting Diode Display Using Printable Elastic Conductors. *Nat. Mater.* **2009**, *8*, 494–499.
8. Someya, T.; Pal, B.; Huang, J.; Katz, H. E. Organic Semiconductor Devices with Enhanced Field and Environmental Responses for Novel Applications. *MRS Bull.* **2008**, *33*, 690–696.
9. Roberts, M. E.; Mannsfeld, S. C. B.; Stoltenberg, R. M.; Bao, Z. Flexible, Plastic Transistor-Based Chemical Sensors. *Org. Electron.* **2009**, *10*, 377–383.
10. Di, C.-A.; Liu, Y.; Yu, G.; Zhu, D. Interface Engineering: An Effective Approach Toward High-Performance Organic Field-Effect Transistors. *Acc. Chem. Res.* **2009**, *42*, 1573–1583.
11. Yoon, M. H.; Kim, C.; Facchetti, A.; Marks, T. J. Gate Dielectric Chemical Structure−Organic Field-Effect Transistor Performance Correlations for Electron, Hole, and Ambipolar Organic Semiconductors. *J. Am. Chem. Soc.* **2006**, *128*, 12851–12869.
12. Becerril, H. A.; Roberts, M. E.; Liu, Z.; Locklin, J.; Bao, Z. High-Performance Organic Thin-Film Transistors through Solution-Sheared Deposition of Small-Molecule Organic Semiconductors. *Adv. Mater.* **2008**, *20*, 2588–2594.
13. Park, S.; Ruoff, R. S. Chemical Methods for the Production of Graphenes. *Nat. Nanothecnol.* **2009**, *4*, 217–224.
14. Allen, M. J.; Tung, V. C.; Kaner, R. B. Honeycomb Carbon: A Review of Graphene. *Chem. Rev.* **2010**, *110*, 132–145.
15. Stankovich, S.; Dikin, D. A.; Dommett, G. H. B.; Kohlhaas, K. M.; Zimney, E. J.; Stach, E. A.; Piner, R. D.; Nguyen, S. T.; Ruoff, R. S. Graphene-Based Composite Materials. *Nature* **2006**, *442*, 282–286.
16. Watcharotone, S.; Dikin, D. A.; Stankovich, S.; Piner, R.; Jung, I.; Dommett, G. H. B.; Evmenenko, G.; Wu, S.-E.; Chen, S.-F.; Liu, C.-P.; *et al.* Graphene−Silica Composite Thin Films as Transparent Conductors. *Nano Lett.* **2007**, *7*, 1888–1892.
17. Berger, C.; Song, Z. M.; Li, X. B.; Wu, X. S.; Brown, N.; Naud, C.; Mayou, D.; Li, T.; Hass, J.; Marchenkov, A. N.; *et al.* Electronic Confinement and Coherence in Patterned Epitaxial Graphene. *Science* **2006**, *312*, 1191–1196.
18. Emtsev, K. V.; Bostwick, A.; Horn, K.; Jobst, J.; Kellogg, G. L.; Ley, L.; McChesney, J. L.; Ohta, T.; Reshanov, S. A.; Rohrl, J.; *et al.* Towards Wafer-Size Graphene Layers by Atmospheric Pressure Graphitization of Silicon Carbide. *Nat. Mater.* **2009**, *8*, 203–207.
19. Reina, A.; Jia, X. T.; Ho, J.; Nezich, D.; Son, H. B.; Bulovic, V.; Dresselhaus, M. S.; Kong, J. Large Area, Few-Layer Graphene Films on Arbitrary Substrates by Chemical Vapor Deposition. *Nano Lett.* **2009**, *9*, 30–35.
20. Di, C.-A.; Wei, D. C.; Yu, G.; Liu, Y. Q.; Guo, Y. L.; Zhu, D. B. Patterned Graphene as Source/Drain Electrodes for Bottom-Contact Organic Field-Effect Transistors. *Adv. Mater.* **2008**, *20*, 3289–3293.
21. Mkhoyan, K. A.; Contryman, A. W.; Silcox, J.; Stewart, D. A.; Eda, G.; Mattevi, C.; Miller, S.; Chhowalla, M. Atomic and Electronic Structure of Graphene-Oxide. *Nano Lett.* **2009**, *9*, 1058–1063.
22. Chen, H.; Muller, M. B.; Gilmore, K. J.; Wallace, G. G.; Li, D. Mechanically Strong, Electrically Conductive, and Biocompatible Graphene Paper. *Adv. Mater.* **2008**, *20*, 3557–3561.
23. Lee, V.; Whittaker, L.; Jaye, C.; Baroudi, K. M.; Fischer, D. A.; Banerjee, S. Large-Area Chemically Modified Graphene Films: Electrophoretic Deposition and Characterization by Soft X-ray Absorption Spectroscopy. *Chem. Mater.* **2009**, *21*, 3905–3916.
24. Eda, G.; Fanchhini, G.; Chhowalla, M. Large-Area Ultrathin Films of Reduced Graphene Oxide as a Transparent and Flexible Electronic Material. *Nat. Nanotechnol.* **2008**, *3*, 270–274.
25. Becerril, H. A.; Mao, J.; Liu, Z.; Stoltenberg, R. M.; Bao, Z.; Chen, Y. Evaluation of Solution-Processed Reduced Graphene Oxide Films as Transparent Conductors. *ACS Nano* **2008**, *2*, 463–470.
26. Schniepp, H. C.; Li, J.-L.; McAllister, M. J.; Sai, H.; Herrera-Alonso, M.; Adamson, D. H.; Prud'homme, R. K.; Car, R.; Saville, D. A.; Aksay, I. A. Functionalized Single Graphene Sheets Derived from Splitting Graphite Oxide. *J. Phys. Chem. B* **2006**, *110*, 8535–8539.

27. Stankovich, S.; Dikin, D. A.; Piner, R. D.; Kohlhaas, K. A.; Kleinhammes, A.; Jia, Y.; Wu, Y.; Nguyen, S. T.; Ruoff, R. S. Synthesis of Graphene-Based Nanosheets *via* Chemical Reduction of Exfoliated Graphite Oxide. *Carbon* **2007**, *45*, 1558–1565.
28. Gómez-Navarro, C.; Weitz, R. T.; Bittner, A. M.; Scolari, M.; Mews, A.; Burghard, M.; Kern, K. Electronic Transport Properties of Individual Chemically Reduced Graphene Oxide Sheets. *Nano Lett.* **2007**, *7*, 3499–3503.
29. Pang, S.; Tsao, H. N.; Feng, X.; Müllen, K. Patterned Graphene Electrodes from Solution-Processed Graphite Oxide Films for Organic Field-Effect Transistors. *Adv. Mater.* **2009**, *21*, 1–4.
30. Wang, X; Zhi, L.-J.; Müllen, K. Transparent, Conductive Graphene Electrodes for Dye-Sensitized Solar Cells. *Nano Lett.* **2008**, *8*, 323–327.
31. Wu, J.; Becerril, H. A.; Bao, Z.; Liu, Z.; Chen, Y.; Peumans, P. Organic Solar Cells With Solution-Processed Graphene Transparent Electrodes. *Appl. Phys. Lett.* **2007**, *92*, 263302.
32. Singh, T. B.; Sariciftci, N. S. Progress in Plastic Electronics Devices. *Ann. Rev. Mater. Res.* **2006**, *36*, 199–230.
33. Newman, C. R.; Frisbie, C. D.; da Silva Filho, D. A.; Brédas, J.-L.; Ewbank, P. C.; Mann, K. R. Introduction to Organic Thin Film Transistors and Design of n-Channel Organic Semiconductors. *Chem. Mater.* **2004**, *16*, 4436–4451.
34. Kim, D. H.; Lee, B.-L.; Moon, H.; Kang, H. M.; Jeong, E. J.; Park, J.-I.; Han, K.-M.; Lee, S.; Yoo, B. W.; Koo, B. W.; *et al.* Liquid-Crystalline Semiconducting Copolymers with Intramolecular Donor-Acceptor Building Blocks for High-Stability Polymer Transistors. *J. Am. Chem. Soc.* **2009**, *131*, 6124–6132.
35. Ito, Y.; Virkar, A. A.; Mannsfeld, S.; Oh, J. H.; Toney, M.; Locklin, J.; Bao, Z. Crystalline Ultrasmooth Self-Assembled Monolayers of Alkylsilanes for Organic Field-Effect Transistors. *J. Am. Chem. Soc.* **2009**, *131*, 9396–9404.
36. Mannsfeld, S. C. B.; Sharei, A.; Liu, S.; Roberts, M. E.; Bao, Z. Highly Efficient Patterning of Organic Single Crystal Transistors from Solution Phase. *Adv. Mater.* **2008**, *20* (21), 4044–4048.
37. Sekitani, T.; Noguchi, Y.; Zschieschang, U.; Klauk, H.; Someya, T. Organic Transistors Manufactured Using Inkjet Technology with Subfemtoliter Accuracy. *Proc. Natl. Acad. Sci. U.S.A.* **2008**, *105*, 4976–4980.
38. Fritz, S. E.; Martin, S. M.; Frisbie, C. D.; Ward, M. D.; Toney, M. F. Structural Characterization of a Pentacene Monolayer on an Amorphous SiO_2 Substrate with Grazing Incidence X-ray Diffraction. *J. Am. Chem. Soc.* **2004**, *126*, 4084–4085.
39. Yoshida, H.; Inaba, K.; Sato, N. X-ray Diffraction Reciprocal Space Mapping Study of the Thin Film Phase of Pentacene. *Appl. Phys. Lett.* **2007**, *90*, 181930.
40. Hu, W. S.; Tao, Y. T.; Hsu, Y. J.; Wei, D. H.; Wu, Y. S. Molecular Orientation of Evaporated Pentacene Films on Gold: Alignment Effect of Self-Assembled Monolayer. *Langmuir* **2005**, *21*, 2260–2266.
41. Puntambekar, K. P.; Pesavento, P. V.; Frisbie, C. D. Surface Potential Profiling and Contact Resistance Measurements on Operating Pentacene Thin-Film Transistors by Kelvin Probe Force Microscopy. *Appl. Phys. Lett.* **2003**, *83*, 5539–5541.
42. Gundlach, D. J.; Zhou, L.; Nichols, J. A.; Jackson, T. N.; Necliudov, P. V.; Shur, M. S. An Experimental Study of Contact Effects in Organic Thin Film Transistors. *J. Appl. Phys.* **2006**, *100*, 024509.
43. Necliudov, P. V.; Shur, M. S.; Gundlach, D. J.; Jackson, T. N. Contact Resistance Extraction in Pentacene Thin Film Transistors. *Solid-State Electron.* **2003**, *47*, 259–262.
44. Klauk, H.; Schmid, G.; Radlik, W.; Weber, W.; Zhou, L.; Sheraw, C. D.; Nichols, J. A.; Jackson, T. N. Contact Resistance in Organic Thin Film Transistors. *Solid-State Electron.* **2003**, *47*, 297–301.
45. Pesavento, P. V.; Puntambekar, K. P.; Frisbie, C. D.; McKeen, J. C.; Ruden, P. P. Film and Contact Resistance in Pentacene Thin-Film Transistors: Dependence on Film Thickness, Electrode Geometry, and Correlation with Hole Mobility. *J. Appl. Phys.* **2006**, 99094504.
46. Miozzo, L.; Yassar, A.; Horowitz, G. Surface Engineering for High Performance Organic Electronic Devices: The Chemical Approach. *J. Mater Chem.* **2010**, *20*, 2513–2538.
47. Koch, N.; Kahn, A.; Ghijsen, J.; Pireaux, J.-J.; Schwartz, J.; Johnson, R. L.; Elschner, A. Conjugated Organic Molecules on Metal *versus* Polymer Electrodes: Demonstration of a Key Energy Level Alignment Mechanism. *Appl. Phys. Lett.* **2003**, *82*, 70–72.
48. Zhang, Y. Y.; Shi, Y.; Chen, F.; Mhaisalkar, S. G.; Li, L. J.; Ong, B. S.; Wu, Y. L. Poly(3,3′′′-didodecylquarterthiophene) Field Effect Transistors with Single-Walled Carbon Nanotube Based Source and Drain Electrodes. *Appl. Phys. Lett.* **2007**, *91*, 223512.
49. Alves, H.; Molinari, A. S.; Xie, H.; Morpurgo, A. F. Metallic Conduction at Organic Charge-Transfer Interfaces. *Nat. Mater.* **2008**, *7*, 574–580.
50. Lee, C.-G.; Park, S.; Ruoff, R. S.; Dodabalapur, A. Integration of Reduced Graphene Oxide into Organic Field-Effect Transistors as Conducting Electrodes and as a Metal Modification Layer. *Appl. Phys. Lett.* **2009**, *95*, 023304.
51. Kaur, I.; Jia, W. L.; Kopreski, R. P.; Selvarasah, S.; Dokmeci, M. R.; Pramanik, C.; McGruer, N. E.; Miller, G. P. Substituent Effects in Pentacenes: Gaining Control over HOMO−LUMO Gaps and Photo-oxidative Resistances. *J. Am. Chem. Soc.* **2008**, *130*, 16274–16286.
52. Videlot-Ackermann, C.; Ackermann, J.; Fages, F. Charge Transfer Effects in Organic Field-Effect Transistors Containing a Donor/Acceptor Heterojunction. *Synth. Met.* **2007**, *157*, 551–557.
53. Amy, F.; Chan, C.; Kahn, A. Polarization at the Gold/Pentacene Interface. *Org. Electron.* **2005**, *6*, 85–91.
54. Chen, W.; Huang, H.; Chen, S.; Huang, Y. L.; Gao, X. Y.; Wee, A. T. S. Molecular Orientation-Dependent Ionization Potential of Organic Thin Films. *Chem. Mater.* **2008**, *20*, 7017–7021.
55. Huang, Y. L.; Chen, W.; Chen, S.; Wee, A. T. S. Low-Temperature Scanning Tunneling Microscopy and Near-Edge X-ray Absorption Fine Structure Investigation of Epitaxial Growth of F_{16}CuPc Thin Films on Graphite. *Appl. Phys. A* **2009**, *95*, 107–111.
56. Hirata, M.; Gotou, T.; Horiuchi, S.; Fujiwara, M.; Ohba, M. Thin-Film Particles of Graphite Oxide 1: High-Yield Synthesis and Flexibility of the Particles. *Carbon* **2004**, *42*, 2929–2937.

Fabrication and Evaluation of Solution-Processed Reduced Graphene Oxide Electrodes for p- and n-Channel Bottom-Contact Organic Thin-Film Transistors

Héctor A. Becerril,[†] *Randall M. Stoltenberg,*[†] *Ming Lee Tang,*[†] *Mark E. Roberts,*[†] *Zunfeng Liu,*[‡] *Yongsheng Chen,*[‡] *Do Hwan Kim,*[§] *Bang-Lin Lee,*[§] *Sangyoon Lee,*[§] *and Zhenan Bao*[†,]*

[†]Department of Chemical Engineering, Stanford University, Stanford, CA 94305 (USA). Department of Chemistry, Brigham Young University-Idaho, Rexburg, ID, 83440 (USA). [‡]Key Laboratory for Functional Polymer Materials and Center for Nanoscale Science and Technology, College of Chemistry, Institute of Polymer Chemistry, Nankai University, Tianjin 300071,(People's Republic of China). [§]Display Laboratory, Materials and Device Institute, Samsung Advanced Institute of Technology, Samsung Electronics CO., LTD., Yongin, 446-712 (Korea).

Address correspondence to zbao@stanford.edu

Supporting Information

Materials used in this study

To evaluate the applicability of our RGO electrodes to organic electronics we chose to work with three different organic semiconductor systems: thermally evaporated pentacene, a p-channel small-molecule semiconductor, thermally evaporated semiconductor copper (II) hexadecafluorophthalocyanine ($F_{16}CuPc$),35 an n-channel semiconductor, and solution-processed

poly(didodecylquaterthiophene-alt-didode-cylbithiazole) (PQTBTz-C_{12}), a p-channel conjugated polymer. The chemical structures of these materials are shown in Figure S1. Thin-films of these materials were deposited onto our RGO electrodes to form BC OTFTs as detailed in the OTFT fabrication and methods sections.

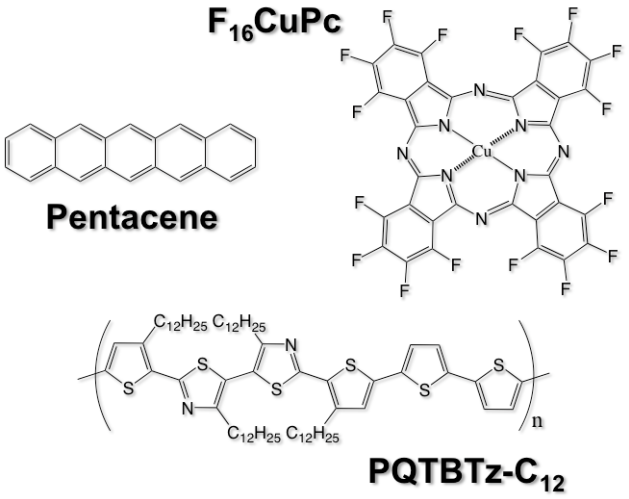

Figure S1. Chemical structures of the organic semiconductors used to explore the material compatibility with RGO electrodes.

Characterization of GO reduction methods

The selection of the reduction method came as a compromise between process cost, process applicability, electrode conductivity and electrode work function. We prepared a large area 21 nm GO film on a SiO_2/Si substrate and cleaved the substrate into four pieces, which were reduced and characterized as indicated in Table S1.

Each fragment was subsequently divided in 2 pieces, and the work function of the material was measured from the first piece. Gold electrodes were deposited on the second piece to perform four-point probe measurements, from which the conductivity of the film was calculated. The results of these measurements, and the comparison to a 40 nm evaporated gold control film are also listed in Table 1. The variation in film conductivity is tremendous, spanning nearly nine orders of magnitude for the graphene-based materials and is highly dependent upon the GO reduction process conditions. The non-

reduced film is an extremely poor conductor. The hydrazine-treated film, which requires a minimum energy investment during the reduction, offers a significantly enhanced conductivity, and the method is compatible with a wide variety of substrate materials since the reduction occurs below 100°C. Unfortunately, the conductivity of this RGO material is still too low for an electrode application. The sample annealed to 400°C is at least seven orders or magnitude more conductive than the non-reduced film, and 10,000 times more conductive than the hydrazine-RGO sample. While the energy required for the reduction is substantial, it is much less than that required for graphitization, and the temperature is still compatible with a number of substrates including glass. The conductivity of the graphitized film is closest to that of the gold control among all the RGO films; however, this value with is still two to three orders of magnitude inferior to gold.

Table 1. Summary of GO Reduction Methods.

Fragment	GO Reduction process	Work Function /eV	Conductivity /Scm^{-1}	Thickness loss
1	None	5.30	7.30×10^{-6}	0%
2	Hydrazine vapor, 18 hr 40 °C	4.83	1.00×10^{-2}	14%
3	Thermal anneal: 3hr, 400 °C, Ar flow.	5.01	7.07×10^{1}	19%
4	Graphitization, 3hr, 1100 °C, 10^{-5} Torr	4.82	2.53×10^{3}	27%
Gold reference	None	4.77	4.52×10^{5}	N/A

The work function of the RGO materials, measured using ultraviolet-photoelectron emission spectroscopy (UPS), appears to be inversely correlated with the conductivity of the film, decreasing significantly from 5.30 eV for the GO film, to 4.82 eV for the graphitized sample. The decrease of the work function is likely due to the gradual disappearance of strongly electronegative oxygenated groups throughout the thickness of the film and to the increasing availability of π-electrons within the film as

the graphene lattice is regenerated. Interestingly, the work function of hydrazine-RGO is rather low, possibly due to the presence of lone-pair electrons from nitrogen atoms incorporated into the RGO film as hydrazones.[Error! Bookmark not defined.] After this analysis we decided to reduce all our GO films using the 400°C thermal annealing method (conductivity ≈71 Scm^{-1}, work function ≈5.01 eV) since it provided a balance of electrode conductivity, work function, energy cost and process applicability. The resistivity of the materials shown in the table is calculated as the inverse of the conductivity and thus, our thermally reduced RGO electrodes (line 3) are about $6.4X10^3$ times more resistive than gold.

Chemical Characterization of the Edges of R-P and P-R RGO Electrodes:

Scanning-electron microscopy (SEM) coupled with Auger electron spectroscopy (AES) was used to probe the composition of the edges of our R-P and P-R RGO electrodes and the results are summarized in Figure S2. We found significant re-oxidation of the RGO electrode sidewalls in the R-P process, with a relatively wide transition region between the gap and the unaffected RGO as determined by AES. This wide transition can be attributed to underetching of the RGO during the plasma treatment, and the result is exacerbated by any physical separation between the etch mask and the RGO film. Deposition of a masking layer directly on the RGO as in the case of Müllen's report,
[1]

can significantly reduce the lateral extent of the undercut but may degrade the surface of the RGO. We therefore avoided the R-P method for device fabrication.

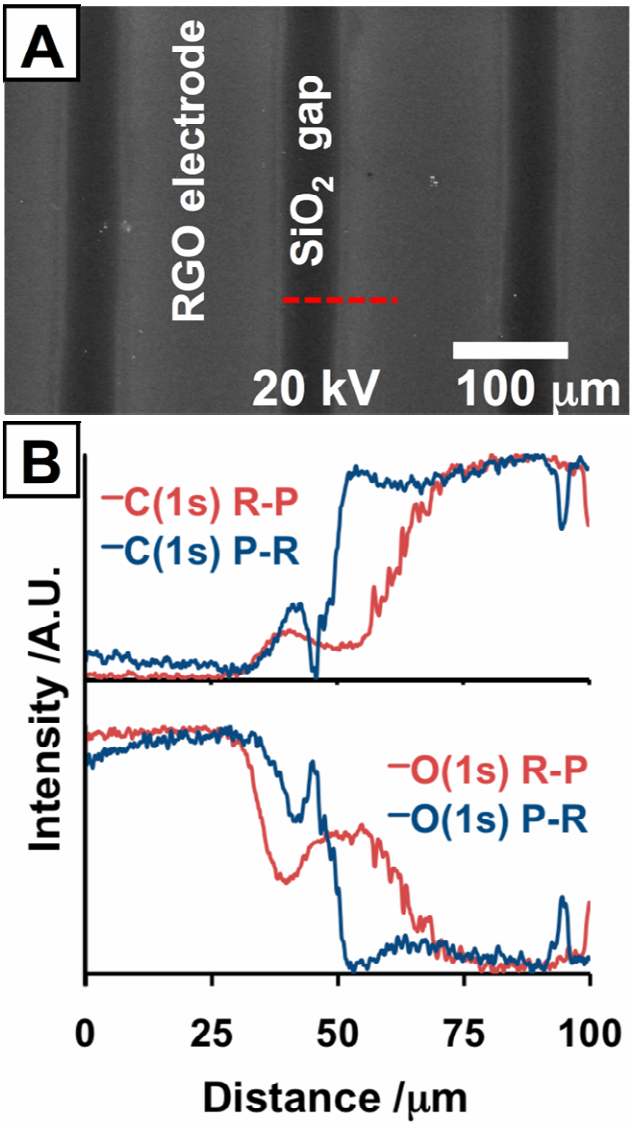

Figure S2. Film composition at the electrode edges for R-P and P-R RGO electrodes. **(A)** SEM micrograph of typical electrodes studied. The RGO and SiO_2 regions are indicated and the gap between electrodes is ≈ 50 μm. The dashed red line indicates the analysis path for collection of AES data shown in **(B-C)** with the position of the edge roughly corresponding to the 50 μm mark. **(B)** Normalized AES carbon (top panel) and oxygen (bottom panel) signals as a function of position for an R-P and a P-R electrode. For carbon the R-P shows a wide transition region between the gap (left) and the electrode (right), while in the P-R the change occurs over about half the distance. Oxygen should only be detectable in the gap (left), but the R-P trace shows a gradual decrease of O_2 signal at the gap/electrode edge with significant oxygen content well into the electrode region (right). The P-R electrodes display a

sharp decrease in O_2 signal narrowly centered about the expected position of the edge.

References

[1] Pang, S.; Tsao, H. N.; Feng, X.; Müllen, K. Patterned Grapehene Electrodes from Solution-Processed Graphite Oxide Films for Organic Field-Effect Transistors. *Adv. Mater.* **2009**, *21*, 1-4.